Santamaría Pérez, D.; Gomis, O.; Pereira, A. L. J.; Vilaplana Cerda, R. I.; Sans, J. A.; Manjón, F. J.; Rodriguez-Hernandez, P.; Muñoz, a.; Ursaki, V.; Tiginyanu, I. M. (2014). Structural and Vibrational Study of Pseudocubic CdIn2Se4 under Compression. Journal of Physical Chemistry C. 118:26987-26999. doi:10.1021/jp5077565.

Structural and Vibrational Study of Pseudocubic $CdIn_2Se_4$ under Compression

David Santamaría-Pérez[1,2,], Oscar Gomis[3], André L.J. Pereira[4], Rosario Vilaplana[3], Catalin Popescu[5], Juan Angel Sans[4], Francisco Javier Manjón[4], Placida Rodríguez-Hernández[6], Alfonso Muñoz[6], Vladislav. V. Ursaki[7], Ion. M. Tiginyanu[7]*

[1] Departamento de Física Aplicada-ICMUV, MALTA Consolider Team, Universidad de Valencia, C/Dr. Moliner 50, Burjassot, 46100 Valencia (Spain)

[2] Earth Sciences Department, University College London, Gower Street, WC1E 6BT, London (UK)

[3] Centro de Tecnologías Físicas: Acústica, Materiales y Astrofísica, MALTA Consolider Team, Universitat Politècnica de València, Camí de Vera s/n, 46022 València (Spain)

[4] Instituto de Diseño para la Fabricación y Producción Automatizada, MALTA Consolider Team, Universitat Politècnica de València, Camí de Vera s/n, 46022 València (Spain)

[5] CELLS-ALBA Synchrotron Light Facility, 08290 Cerdanyola del Vallés, Barcelona (Spain)

[6] Departamento de Física, Instituto Univ. de Materiales y Nanotecnología, MALTA Consolider Team,, Universidad de La Laguna, La Laguna, Tenerife (Spain)

[7] Institute of Electronic Engineering and Nanotechnologies, Academy of Sciences of Moldova, 2028 Chisinau (Moldova)

ABSTRACT

We report a comprehensive experimental and theoretical study of the structural and vibrational properties of α-$CdIn_2Se_4$ under compression. Angle-dispersive synchrotron x-ray diffraction and Raman spectroscopy evidence that this ordered-vacancy compound with pseudocubic structure undergoes a phase transition (7 GPa) towards a disordered rocksalt structure as observed in many other ordered-vacancy compounds. The equation of state and the pressure dependence of the Raman-active modes of this semiconductor have been determined and compared both to *ab initio* total-energy and lattice dynamics calculations and to related compounds. Interestingly, on decreasing pressure, at ~ 2 GPa, $CdIn_2Se_4$ transforms into a spinel structure which, according to calculations, is energetically competitive with the initial pseudocubic phase. The phase behaviour of this compound under compression and the structural and compressibility trends in AB_2Se_4 selenides are discussed.

KEYWORDS: ordered vacancy compounds, phase transition, high pressure, pseudocubic, X-ray diffraction, Raman, ab initio calculations

INTRODUCTION

Ternary adamantine $A^{II}B^{III}{}_2X_4$ semiconductors have been extensively investigated in the last 30 years mainly because they are tetrahedrally-coordinated ordered-vacancy compounds (OVCs) derived from the zincblende (ZB) structure whose behaviour locates them as a bridge between crystal and impurity physics[1]. In these OVCs, only three quarters of the ZB cation sites are filled

leaving one vacant site per formula unit. This stoichiometric atomic-vacancy arrangement leads to tetragonal structures instead of cubic ones that provide to these compounds interesting optical and structural properties such as nonlinear-optic characteristics and order-disorder transitions[1-3]. Particularly, studies of structural transformations of these semiconductors at high-pressure (HP) conditions have received increasing attention in the last years[4-31], leading to systematics in compressibility and pressure - composition phase boundaries. It has been found that these semiconductors usually crystallize in tetragonal structures like defect chalcopyrite (DC) [space group (S.G.) *I-4,* No. 82, *Z*=2] and defect stannite (DS) [S.G. *I-42m,* No. 121, *Z*=2]. The behaviour of these structures at high pressures has been reviewed in several chapters[32-34] of a recent monograph.

$CdIn_2Se_4$ is an OVC whose structural and vibrational properties have been thoroughly studied at ambient conditions. X-ray diffraction (XRD) measurements have evidenced that $CdIn_2Se_4$ shows structural polytypism as its tetragonal cell has been reported with at least three different *c/a* values of 1, 2 and 4, which correspond to the α, β and γ phases, respectively[1, 35-38]. The different modifications can be obtained depending upon transport conditions during the crystal growth[36]. The common α phase crystallizes in a tetragonal pseudocubic (PS) structure; therefore, α-$CdIn_2Se_4$ will be hereon noted as PS-$CdIn_2Se_4$. The structures of the β and γ phases are still unknown despite a structure similar to the DC phase has been proposed for the β phase[38]. On the other hand, the vibrational properties of PS-$CdIn_2Se_4$ at ambient conditions have been studied by means of Raman scattering and Infrared spectroscopy and many similarities with the vibrational modes of the ZB structure have been found[39-42].

The structural relationship between the ZB (**Fig. 1a**) and PS (**Fig. 1b**) structures of $CdIn_2Se_4$ can be easily illustrated using a simple Bärnighausen-tree[43] (see **Fig. 2**). One starts with the

highly symmetrical ZB structure [S.G. *F*-43*m*, No. 216, Z=4], the aristotype, at the top of the tree and sets up group–subgroup relations that lead into the space group of PS-$CdIn_2Se_4$ [S.G. *P*-42*m*, No. 111, Z=1]. The lattice parameters and atomic coordinates of both phases are indicated in **Fig. 2**. In our case, an intermediate structure with S.G. *P*-43*m,* No. 215, Z=4 was defined. Every step of symmetry reduction causes that the Wyckoff positions occupied with cations loose site symmetry and split into symmetrically independent positions. In addition, atomic coordinates of Se atoms coupled by symmetry *(x,x,x)* become independent *(x,x,z)*. In summary, the lattice transformations shown in **Fig. 2** make possible that the *P*-42*m* space group could define more complex stoichiometries: (i) The splitting of Wyckoff positions permits the substitution with atoms of different elements and also to leave vacant a fraction of the cation positions, and (ii) the site-symmetry reduction permits distortions; i.e. the coordinates of the Se atoms can deviate from the ideal positions of the undistorted ZB structure.

The phase behaviour of PS-$CdIn_2Se_4$ under compression was studied at high temperatures and a phase transition to the spinel structure was found above 1 GPa for temperatures higher than 380ºC[44,45]; an observation which seems to be in agreement with available theoretical *ab initio* calculations[46]. However, the pressure dependence of the structural and vibrational properties of PS-$CdIn_2Se_4$ have not been addressed yet, except for some theoretical aspects recently reported[34]. The present work is devoted to the investigation of the structural and vibrational behaviour of this OVC under high pressure at room temperature. Tuning the thermodynamic variable pressure, we envisage to transform the initial ordered PS phase into a disordered cationic structure, which could be recovered at ambient conditions after compression, as observed in some previous studies on OVC materials[9,15-18,23]. *In situ* angle-dispersive XRD and Raman measurements were performed up to 17 GPa and downstroke to ambient conditions. Our

experimental results are compared to *ab initio* total energy calculations. We will also present a comparative analysis on the light of previous structural studies of OVCs under pressure, which will show polymorphism and compressibility trends depending on composition and pressure.

EXPERIMENTAL DETAILS

Stoichiometric single crystals of PS-$CdIn_2Se_4$ were grown by chemical vapor transport method using iodine as a transport agent[47]. A quartz ampoule was loaded with cadmium, indium and selenium in stoichiometric ratio together with 5 mg/cm^3 iodine. The ampoules were evacuated to 10^{-5} torr, sealed off, and placed in a horizontal double-zone furnace with source temperature of 720°C and deposition temperature of 670°C. The growth process lasted 100 hours. Chemical and structural analyses showed the stoichiometric composition of the crystals and no spurious phases were observed. Ambient pressure XRD and Raman scattering measurements confirmed that our sample has the previously reported pseudocubic *P-42m* structure.

Angle-dispersive powder HP-XRD measurements at room temperature were performed up to 15 GPa at beamline BL04-MSPD of the Spanish ALBA synchrotron light source[48] using a monochromatic beam (λ = 0.4246 Å) with a beam diameter of 20 μm full-width at half maximum. XRD images were collected using a MARCCD detector located at 230 mm away from the sample and then integrated and corrected for distortions using FIT2D[49]. The typical acquisition time was 10 s. For HP-XRD measurements, PS-$CdIn_2Se_4$ powder sample was placed in a 150-μm-diameter 45-μm-thick hole of a stainless-steel gasket inside a membrane diamond anvil cell which allowed access to an angular range of $2\theta \sim [0\text{-}18°]$. A mixture of 16:3:1 methanol:ethanol:water was used as pressure-transmitting medium which behaves in a quasi-

hydrostatic way up to 10.5 GPa[50]. Cu was used as an internal pressure gauge[51]. The indexing and refinement of the powder patterns were performed using the Chekcell[52], Powdercell[53] and Fullprof[54] program packages.

Unpolarized HP-Raman scattering measurements at room temperature were performed on powder and single crystal samples in backscattering geometry with a LabRAM HR UV microspectrometer coupled to a Peltier-cooled charge couple device camera. A 632.81 nm (1.96 eV) HeNe laser excitation line with a power around 1 mW and a spectral resolution better than 2 cm^{-1} were used. In order to analyze the Raman spectra, the peaks have been fitted to a Voigt profile (Lorentzian profile convoluted by a Gaussian profile) where the spectrometer resolution is taken as a fixed Gaussian width (1.5 cm^{-1}). For HP-Raman measurements, PS-$CdIn_2Se_4$ samples were loaded in the same cell with a 16:3:1 methanol:ethanol:water mixture as pressure-transmitting medium and the ruby fluorescence scale was used for pressure calibration[55].

During HP-Raman experiments, samples were checked by visual inspection before and after each measurement and by monitoring the time dependence of the Raman signal at different accumulations and at different sites with different laser powers to be sure that no heating effects occur during the measurements by the incoming laser excitation. Note that the laser energy is above the band gap energy of $CdIn_2Se_4$ with an indirect band gap energy of 1.55 eV and a direct band gap energy of 1.67 eV[56] measured at ambient conditions**.** We have noted that under strong laser excitation (>10 mW) at high pressures the sample tends to decompose due to severe laser heating (see supplementary material). This result clearly stresses the importance of performing Raman scattering measurements in chalcogenides under low excitation conditions, even at high pressures where thermal transfer processes due to contact of the sample with a pressure-transmitting medium and diamonds are enhanced.

COMPUTATIONAL DETAILS

Ab initio total-energy calculations on the initial pseudocubic P-42m and the spinel (S.G. Fd-3m, No. 227, Z=8) structures were performed within the density functional theory (DFT)[57] using the plane-wave method and the pseudopotential theory with the Vienna *ab initio* simulation package (VASP)[58-61]. The projector-augmented wave scheme[62,63] implemented in this package was used to take into account the full nodal character of the all-electron charge density in the core region. Basis sets including plane waves up to an energy cutoff of 370 eV were used to achieve highly converged results and an accurate description of the electronic properties. The exchange-correlation energy was taken in the generalized gradient approximation (GGA) with the PBEsol exchange-correlation prescription[64]. A dense special k-points sampling ((8,8,8) mesh) for the Brillouin zone integration was selected in order to obtain very well-converged energies and forces. At each selected volume, the structures were fully relaxed to their equilibrium configuration through the calculation of the forces and the stress tensor. In the relaxed equilibrium configuration, the forces on the atoms were found to be smaller than 0.004 eV/Å and the deviation of the stress tensor from a diagonal hydrostatic form was found to be smaller than 1-2 kbar.

The DFT method allows obtaining a set of energy and volume data for a selected structure. Pressure, like other energy derivatives, is obtained at the same time from the stress tensor[65]**.** From the values of energy, volume, and pressure, the enthalpy of each structure was calculated to determine the most stable phase among those considered at each pressure and zero temperature (zero-point motion effects were not included). Using the enthalpy difference taking as a reference the low-pressure phase, one can obtain the theoretical phase transition pressure.

E-V data for the disordered rocksalt (DR) structure (S.G. *Fm*-3*m*, No. 225, Z=1) of $CdIn_2Se_4$ were calculated using a lower symmetry structure (S.G. *Imma*, No. 74, Z=4), which allows leaving vacant ¼ of the cationic positions, while the remaining ¾ fraction is occupied (see the lattice parameters and atomic coordinates used for describing the DR structure in **Table I**). The definition DR structure with a *Imma* structure can be derived by group-subgroup relationships in the following way: (i) the description of the DR (No. 225) phase with lattice parameter a ~ 5.5 Å using a supergroup (No. 227) with a larger cell (a'=2a ~ 11 Å), and (ii) the subsequent description of the lattice using a orthorhombic subgroup *Imma* (No. 74) with lattice parameters a'' = b'' = a'/sqrt(2)= 7.77 Å and c'' = a' = 11 Å [66]. In order to describe an ideal DR structure, the lattice parameters of the Imma structure ought to have the above values and Se atoms should be located at fixed positions 8h (0, y = 0, z = ¼) and 8i (x = ¼, ¼, z = 0). Unfortunately, the simulation of such an orthorhombic structure shows non-negligible forces on the atoms what leads to the deviation of the stress tensor from a diagonal hydrostatic form. Nevertheless, the full relaxation of all the three lattice parameters plus the (0, y, z) and (x, ¼, z) coordinates of the Se atoms, give values very close to those of the ideal cubic DR structure (see **Table I**).

Lattice-dynamics calculations of phonon modes were performed at the zone centre (Γ point) of the Brillouin zone. Highly converged results on forces are required for the calculation of the dynamical matrix using the direct force constant approach (or supercell method)[67]**.** The construction of the dynamical matrix at the Γ point of the Brillouin zone involves separate calculations of the forces in which a fixed displacement from the equilibrium configuration of the atoms within the primitive cell is considered. The number of such independent displacements in the analyzed structures is reduced due to the crystal symmetry. Diagonalization of the dynamical matrix provides the frequencies of the normal modes. Moreover, these calculations

provide information about the symmetry of the modes and their polarization vectors and allow us to identify the irreducible representations and the character of the phonon modes at the Γ point.

In order to include the LO-TO splitting in our study, we use a supercell to add the effect of the electric field, which is not directly taken into account by the force-constant direct method. To obtain the LO-TO splitting we have to add these effects, because these term is non-analytical at the Γ point, which depends on the Born effective charge tensors and the electronic dielectric constant. Thus, the pure *B* and *E* modes with TO and LO splitting can be calculated.

RESULTS

A. CRYSTAL STRUCTURE UNDER COMPRESSION

Figure 3 shows a selection of our XRD powder data for $CdIn_2Se_4$ at several pressures. At ambient conditions, the XRD pattern corresponds to the tetragonal pseudocubic *P*-42*m* phase previously reported in the literature[68], with similar lattice parameters: a = c = 5.8185(2) Å, and comparable Se coordinates (0.284(2), 0.284(2), 0.243(3)), as obtained from our Rietveld refinement shown at the bottom of Fig. 3. XRD patterns can be indexed with the initial PS phase up to 7 GPa. Above this pressure, additional diffraction peaks appear (see arrows in **Fig. 3**) which clearly indicates the existence of a pressure-induced phase transition in $CdIn_2Se_4$.

Upon further compression, the peaks of the low-pressure phase disappear completely at 8.7 GPa. At this pressure, XRD peaks can be indexed with a cubic unit-cell with lattice constant: a = 5.362(16) Å; thus accounting for an approximated volume collapse of ~ 8.7% at the phase transition. This HP phase is stable up to the maximum pressure reached in this study (15 GPa). The intensities of the Bragg peaks are in good agreement with a DR structure (see **Fig. 1c**),

where the vacant, the Cd atom and the two In atoms per unit-cell are randomly distributed within a fcc net which is interwoven with a fcc Se lattice (all atoms are octahedrally coordinated). As a consequence of the disorder caused by the phase transition and the vicinity of the loss of the quasi-hydrostatic conditions at a pressure of 8.7 GPa, the Bragg maxima of this phase are significantly broader than those of the low-pressure phase. The calculated profile for the DR phase after Rietveld refinement is shown in **Fig. 3**. The PS-to-DR transition was expected in $CdIn_2Se_4$ because a similar structural sequence from a tetrahedrally-coordinated tetragonal phase to an octahedrally-coordinated cubic phase has been reported for many OVCs under compression, indicating that an order-disorder process occurs when pressure is applied to AB_2X_4 chalcogenides[9,16-18,23,29,30]. The DR phase is stable during decompression down to ~2.7 GPa. Below this pressure, new broad peaks appear in the XRD patterns (see **Fig. 3**). According to the position of the new XRD peaks, the retrieved structure could correspond to the spinel phase, which was experimentally observed in $CdIn_2Se_4$ and other OVCs after a HP/high-temperature treatment[44,45]. Additionally, it must be stressed that the spinel phase has been metastably found on decompression from the DR phase in $CdAl_2S_4$ in a very recent HP study at ambient temperature near 1 atm[31]. Note that the relative intensity of the new peaks increases as pressure gradually decreases, showing a coexistence region of DR and spinel phases between 2 and 0.3 GPa. Since both phases are cubic phases and some peaks overlap, we have no certainty of a complete transformation to the spinel structure at 1 atm. However, intensities of the XRD peaks which correspond to the recovered sample (see top of **Fig. 3**) seem to present a relative good agreement with those of a single spinel phase (see vertical red marks at the top of **Fig. 3**).

XRD measurements carried out in this static compression study only show the existence of the spinel structure below 2.7 GPa in the decompression process, after the sample had previously

transformed into the DR structure and had increased the coordination number of the metallic atoms from 4 in the initial PS phase to 6. Therefore, the relocation of cations into tetrahedral voids seems to be favoured once all of them have achieved the six-fold coordination. This fact makes sense since the DR structure can be described in the same space group as the spinel (see Computational details Section) and the phase transition could consist of a progressive displacement of the Cd atoms in octahedral sites to tetrahedral sites. This migration would correspond to a displacement of ~2 Å along the diagonal of the *Fd*-3*m* cube[66]. Thus, XRD data points between 2 GPa and 0.3 GPa in downstroke (see **Fig. 4**) could be considered both, a coexistence of the DR and spinel phases or just an intermediate structure with incomplete atom migration.

The evolution observed for the unit-cell volume of the different phases is shown in **Fig. 4**. The variation of the volume with pressure has been fitted to a second-order Birch–Murnaghan equation of state (EOS)[69], where the values of the bulk modulus (B_0) and the unit-cell volume at zero pressure (V_0) are left to vary freely. The characteristic EOS parameters obtained for the different polymorphs are collected in **Table II**. A good agreement is found between the experimental values and those obtained from *ab initio* calculations. We note that B_0 = 41.1(9) GPa obtained experimentally for PS-$CdIn_2Se_4$ is also similar to that obtained for other OVCs (see **Table III**) with tetragonal structures like defect chalcopyrite or defect stannite. The low value of B_0 is ascribed to the presence of the stoichiometric vacancies in the structure of OVCs which governs the compressibility of this kind of compounds[24]. On the other hand, the B_0 value obtained theoretically for the spinel-type phase of $CdIn_2Se_4$ (63.9(3) GPa) is about 70% greater than that obtained theoretically for the PS phase. The larger bulk modulus for the spinel phase than for the PS phase in $CdIn_2Se_4$ is in agreement with the cation coordination increase from the

PS phase with tetrahedral coordination and cation coordination numbers 4:4 to the spinel phase with tetrahedral and octahedral coordination and cation coordinations 4:6 for Cd and In, respectively. Finally, we must note that our calculated data are more consistent that those reported by Marinelli et al.[46] for the PS and spinel structures (see **Table II**) when compared to experimental data. These authors used the local density approximation (LDA) instead of the general gradient approximation (GGA) in their simulations and, consequently, their unit-cell volumes (bulk moduli) are underestimated (overestimated) with respect to experimental ones.

The values for B_0 and B_0' for PS-$CdIn_2Se_4$ and other OVC with DC or DS structure are summarized in **Table III** for the sake of comparison. Larger values of the bulk modulus at zero pressure are expected for sulfide-based OVCs than for selenide-based OVCs due to the larger ionic radio of selenium in comparison to that of sulphur. On the other hand, it is also expected the decrease of the bulk modulus of selenides on the increase of the ionic radius of the *A* and *B* cations. However the values for B_0, and B_0' reported in **Table III** do not always agree with the expected results when comparing data from different compounds and experiments. There are at least two reasons for this: (i) The values of B_0 and B_0' are strongly correlated in the way that the increment of one implies the decrement of the other one, and (ii) Compressibility strongly depends on the hydrostatic conditions of the XRD experiment. In this sense, previous works have shown an overestimation of B_0 under non-hydrostatic conditions[23,24,71]. These two facts make difficult in practice to compare results for B_0 obtained in different experiments by different authors, particularly when difference between B_0 values seems to be not very large. In any case, experimental results confirm the high compressibility of tetrahedrally-coordinated OVCs.

In order to better understand how the structure of PS-$CdIn_2Se_4$ behaves under compression we plotted in **Fig. 5(a)** the theoretical pressure dependence of the cation-anion and vacancy-

anion distances of this compound. A good agreement is found between the calculated and experimental distances at 1 atm. The largest distance is that of Cd-Se, the intermediate distance that of In-Se, and the shortest distance is that of vacancy-Se. Cd-Se and In-Se distances are much less compressible than the vacancy-Se distance, despite the latter is the smallest one. The high compressibility of the vacancy-Se distance is due to the weak repulsion between the separated electron distributions of Se atoms surrounding the vacancy. Consequently, Se atoms move towards the vacancy site at a faster rate than to the sites occupied by cations. For completeness, **Fig. 5(b)** shows the compressibility of the cation-anion and vacancy-anion internal distances for PS-$CdIn_2Se_4$ as a function of pressure. The distance compressibility decreases following the sequence "vacancy-Se > Cd-Se > In-Se". At HP, the compressibility of the two cation-anion distances tends to approach to a similar value whilst the vacancy-Se distance compressibility is still much larger. The calculated compressibility at room pressure for the In-Se, Cd-Se, and vacancy-Se distances are $3.8 \cdot 10^{-3}$ GPa^{-1}, $5.9 \cdot 10^{-3}$ GPa^{-1}, and $25.2 \cdot 10^{-3}$ GPa^{-1}, respectively.

B. LATTICE DYNAMICS UNDER COMPRESSION

According to group theory[72], the pseudocubic structure of $CdIn_2Se_4$ has 21 normal vibrational modes at the centre of the Brillouin zone with the mechanical representation given by:

$$\Gamma_{21} = 2A_1\,(R) \oplus 2A_2\,(IA) \oplus 1B_1\,(R) \oplus 3B_2\,(R, IR) \oplus 5E\,(R,IR) \oplus B_2 \oplus E$$

where R means Raman active, IR infrared active and IA optically inactive (silent mode). The B_2 and E are polar modes, with E modes being doubly degenerated, and three modes (B_2 + E) are acoustic ones. Additionally, two modes should be observed for each B_2 and E modes, due to the

transversal-longitudinal optic (TO-LO) splitting of the polar modes. Consequently, taking into account the TO-LO splitting, up to 19 Raman-active modes and 13 IR-active modes could be observed in the PS phase.

Figure 6 shows the theoretical phonon dispersion curves in PS-$CdIn_2Se_4$ along different symmetry points of the Brillouin zone and the corresponding total and atom-projected phonon density of states. This figure allows one to divide the vibrational spectrum, like in other AB_2X_4 OVCs, mainly into two regions: (i) the low-frequency region below 120 cm^{-1}, and (ii) the high-frequency region above 120 cm^{-1}. Consequently, the Raman spectrum can be divided into these two regions. This result is in contrast with most OVCs showing tetragonal DC or DS structures where three regions have been observed[26,27,31]. In the low-frequency region, there are two E, one B_2 and one A_2 phonons while in the high-frequency region there are two A_1, one A_2, two B_2 and one B_1 phonons. The one-phonon density of states shows that while Cd atoms contribute mainly to the vibrations below 70 cm^{-1} and between 150 and 200cm^{-1}, Se and In atoms contribute in the whole vibrational spectrum. The only region where there is only contribution to Se atoms is the region near 133 cm^{-1} which corresponds to the A_1^1 phonon; i.e., the most intense phonon in the Raman spectrum corresponding to the breathing mode of the vacancy which is typical of AB_2X_4 OVCs. In the high-frequency region above 200 cm^{-1}, the vibrations involve only In and Se atoms, thus suggesting that these vibrations are In-Se bond stretching and bond bending modes of the tetrahedron formed by Se anions and In cations. The study of the atomic vibrations was further corroborated with J-ICE software[73], which allows one to get images of the atoms participating in the different vibrational modes.

Figure 7(a) shows unpolarized Raman spectra of PS-$CdIn_2Se_4$ at different pressures up to 17.1 GPa at 298 K. Our Raman spectrum measured at 1 atm shows similar features to those

observed in a previous Raman work which reported 12 Raman modes[41,42]**.** All Raman modes disappear at pressures above 6.4 GPa, thus indicating a HP phase transition to a Raman-inactive phase which can be attributed to a DR structure as observed in our XRD measurements. At the top of **Figure 7(a)** we show the Raman spectrum measured at 1 atm after releasing pressure. The lack of Raman peaks in that spectrum indicates that the PS-to-DR phase transition is irreversible. This contrasts with the result found with HP-XRD measurements where a spinel-type phase is found in coexistence with the DR structure after releasing pressure at 1 atm. At present, the cause for this discrepancy is unknown since XRD measurements have been performed with powder samples and Raman scattering measurements have been performed both with single crystal and powder samples. Besides, Raman measurements have been performed in samples moderately heated near ambient pressure with the excitation laser. In none of these cases we were able to detect any signal that could be attributed to the spinel phase. The only possibility to match XRD and Raman results on downstroke is to consider that the spinel phase is not well crystallized and it displays a very weak Raman signal that it cannot be detected despite part of the sample is already in the spinel phase. In this respect, we have to stress that rather broad Raman signal corresponding of the spinel phase was recently reported for $CdAl_2S_4$[31]. In fact, the experimental frequencies and pressure coefficients of this phase do not fit perfect with theoretical results likely due to the bad crystallization of the spinel phase on decreasing pressure from the DR phase. Note that the DR-to-spinel phase transition is a disorder-to-order transition and so perfect recovery of the spinel phase is unlikely unless some thermal energy is provided to the system.

The Raman spectrum of PS-$CdIn_2Se_4$ at ambient pressure is characterized by two strong modes: i) the A_1^1 mode near 140 cm^{-1}, which corresponds to the symmetric stretching of vacancy-Se tetrahedra and known as the breathing mode of the vacancy, and ii) the highest

frequency mode near 230 cm^{-1} with mixed B_2 and E character (see **Table IV and Fig. 7(b)**)[41,42]. It must be stressed that there is a correlation between the phonons of the DS and PS phases. The only difference between the vibrational modes of both phases is the presence of a Raman-active B_1 mode (contributed by atoms in 4d Wyckoff sites) in the DS structure which becomes a Raman-inactive A_2 mode (contributed by atoms in 2f Wyckoff sites) in the PS structure[72]. In particular, we have found that the typical A^2 mode, which is present in the Raman spectrum of the DC structure of OVCs [26,27], has A_2 symmetry (which is inactive) in the DS and PS structures and therefore it is absent in the Raman spectrum of these two phases[26,27] so its appearance or disappearance in several OVCs has been claimed in many cases as a signature of a phase transition[22,27,28].

We have followed experimentally the pressure dependence of 8 Raman modes of PS-$CdIn_2Se_4$ up to 6.5 GPa. The pressure dependence of the Raman-mode frequencies are depicted with symbols in **Fig. 7(b)**. For comparison with our measurements and in order to help in the identification of the different symmetries of the first-order Raman modes, we plotted with lines in **Fig. 7(b)** the theoretical pressure dependence of the Raman modes with pure A_1-, A_2-, B_1-, B_2-, and E-symmetry, where TO and LO splitting for B_2 and E polar modes are noted with solid and dashed lines, respectively. All Raman modes of the low-frequency region show negative pressure coefficients while those of the high-frequency region display positive pressure coefficients. This feature is similar to the Raman modes in other OVCs with DC or DS structure and their significance has been previously discussed[28,31].

Table IV summarizes the experimental and theoretical zero-pressure frequencies, and pressure coefficients for the vibrational modes of PS-$CdIn_2Se_4$. Furthermore, we have tentatively assigned the symmetries of the Raman peaks on the basis of our experimental and theoretical

results (see **Table IV**). A comparison with previous works[39-42] evidences that our symmetry assignment of Raman-active modes is more consistent because it is based on the pressure dependence of the frequency of the different modes and on the comparison of our frequencies and pressure coefficients to theoretical calculations while previous works could barely distinguish between different symmetries because of the lack of sensitivity to polarization of indium based compounds[41,42]. Our symmetry assignments agree with those of previous works only for the strongest modes; i.e., the vacancy breathing mode A_1 near 140 cm^{-1} and the mode of highest frequency, which is usually attributed in the literature to a mixture of bands with E^5(LO) and B_2^3(LO) character[39-42]. The main difference of our work with respect to previous works is that we have observed that this last mode exhibits a double structure with very different pressure coefficients; thus, we have attributed one of the components to the E^5 (LO) mode and another to the B_2^3 (LO) mode. However, since our Raman measurements are not polarized and the bands corresponding to TO modes have not been observed, we cannot discard a mixture of E^5 (TO+LO) and a mixture of B_2^3 (TO+LO) in these high-frequency modes since they are broad modes and the calculated TO-LO splitting is only around 10 cm^{-1} in both cases.

As regards other Raman modes, the double structure below 200 cm^{-1} at 1 atm exhibits a pressure dependence that can be better modelled with three bands which have been attributed to the E^3 (TO+LO), E^4 (TO) and A_1^2 + B_1 modes. Our calculations show that three of these four modes are almost degenerate in frequency but show different pressure coefficients that we have used to distinguish between them. Finally, Raman modes at lower frequencies can be clearly assigned because of the close matching between the frequencies and pressure coefficients between our measurements and calculations.

C. STRUCTURAL FIRST-PRINCIPLES CALCULATIONS UNDER COMPRESSION

Total-energy (E) calculations as a function of volume (V) were performed for the PS, DR and spinel structures of $CdIn_2Se_4$. Calculated structural parameters are in good agreement with experimental values (hereafter in parentheses for the sake of comparison), as shown in **Fig. 4** and **Table II**. From the enthalpy-pressure curves performed using GGA-PBEsol prescription (see **Fig. 8**), several important features can be inferred

(i) Our calculations at T=0 K show that at ambient pressure the spinel phase is more stable than the PS phase. These results contrast with those of Marinelli et al., who used the local density approximation (LDA), and found the PS phase to be more stable than the spinel phase at ambient conditions[46]. This difference is understood by the underestimation (overestimation) of the volumes with respect to the experimental results when using LDA (GGA). In the case of GGA-PBEsol, there is a very slight underestimation of the volume so that the calculations yield a more stable the spinel phase than the PS phase. Since all these calculations are performed at T=0 K, we can state that the PS and spinel structures at 1 atm differ only a few meV in energy and, therefore, they are energetically competitive within error margins. In this regard, it is important to highlight that the equilibrium PS molar volume is 6.5 (7.2)% larger than that of the spinel. A similar result was found in Ref. 46**.** These theoretical results, together with experimental observations, provide evidence of a complex energy landscape for $CdIn_2Se_4$ with two similar-depth local minima for spinel and PS structures and show that static compression could be used as a tool for overcoming activation barriers and obtaining novel stable polymorphs.

(ii) Upon compression, theoretical calculations confirm a phase transition to a DR phase which is simulated by a Imma (S.G. 74) structure. Both the PS and spinel structures

would transform into this HP phase at 4.9 GPa and 7.3 GPa, respectively, in relatively good agreement with experimental data, where the phase transition occurs at 7 GPa. This structural rearrangement implies a volume collapse of 9.5 (8.6)% and 7.3 (4.5)% respect to the PS and spinel phases, respectively.

We want to highlight that the phase diagram of $CdIn_2Se_4$ below 4 GPa and 600 °C was previously determined by Range[45]. No structural transformation was reported below 360°C in good agreement with our data, and attributed it to kinetic hindrance. The spinel structure was found after quenching the $CdIn_2Se_4$ sample from 1 GPa and 380 °C. At similar pressures and temperatures above 500 °C the spinel transforms into a DR-type structure. It is interesting to remark that the same structural sequence is observed at moderate pressures (P = 1-2 GPa) by increasing temperature[45] and at ambient temperature by a largest increase of pressure (P> 7 GPa) as shown in this work.

The stability closeness of both PS and spinel structures in $CdIn_2Se_4$ at ambient conditions is supported by the diagrammatic sorting of the AB_2X_4 group of compounds. Muller and Roy[74] and, more recently, Zhang and Zunger[75] constructed diagrams whose coordinates were the Shannon-Prewitt crystal radii and the Zunger nonlocal pseudopotential orbital radii of A and B atoms, respectively. These maps were capable of systematizing and predicting the crystal structures of compounds with the aforementioned stoichiometry with a high success rate (96 and 98%, respectively, for anion dependent maps). In particular, it was found that 129 Se compounds of 132 were properly located in their map within their structural-type regions[75]. According to Zhang and Zunger diagram shown in their Fig. 2b [75], $CdIn_2Se_4$ is placed in the borderline between the PS and the spinel region in good agreement with experimental and theoretical data. It is

interesting to note that the Cr_3S_4-type structure region overlaps with that of the spinel, but the former is only formed when both A and B cations are transition metal elements.

CONCLUSIONS

Unlike other OVCs, which usually crystallize in the tetragonal DC or DS structures, $CdIn_2Se_4$ is a unique OVC crystallizing in the tetragonal PS structure. We have reported a study of the structural and vibrational properties of PS-$CdIn_2Se_4$ under high pressure at ambient temperature and have found that:

i) Its bulk modulus is similar to those of other selenide-based OVCs like $CdGa_2Se_4$ and $HgGa_2Se_4$.

ii) The compression of its bond distances is similar to that of other selenide OVCs like $HgGa_2Se_4$.

iii) Its Raman spectrum is different from that of other OVCs with DC or DS structure but the vibrations show considerable similarities, especially with the DS structure.

iv) It undergoes a pressure-induced phase transition towards a DR structure above 7 GPa as many of the AB_2X_4 OVCs, but it undergoes a phase transition towards the spinel structure on decreasing pressure unlike many OVCs and similarly to $CdAl_2S_4$.

v) It suffers a pressure-induced decomposition at pressures close to the PS to DR phase transition pressure under strong laser heating. This is likely due to the decrease of the bandgap at high pressures which leads to major absorption of the laser radiation resulting in a sample decomposition as evidenced by the observation of trigonal Se in a similar way as recently found in $HgGa_2Se_4$ and other binary chalcogenides (see

Supplementary material). Therefore, our work points to the need of extremely careful Raman measurements at low excitation conditions when studying chalcogenide materials at high pressures.

We hope the present work will foster new high-pressure studies of OVCs with spinel structure in order to establish a closer relationship between these two types of structures in AB_2X_4 compounds.

AUTHOR INFORMATION

Corresponding Author

*Dr. David Santamaria-Perez. Email: d.santamaria-perez@ucl.ac.uk

Phone: +34 963543881

Present Address

[2] Earth Sciences Department, University College London, Gower Street, WC1E 6BT, London, (UK)

Author Contributions

The manuscript was written through contributions of all authors. All authors have given approval to the final version of the manuscript.

ABBREVIATIONS

OVC, ordered-vacancy compound; ZB, zincblende; HP, high-pressure; DC, defect-chalcopyrite; S.G., space group; DS, defect-stannite; XRD, x-ray diffraction; PS, pseudocubic; DFT, density functional theory; GGA, generalized gradient approximation; DR, disordered rocksalt; E, energy; V, volume.

ACKNOWLEDGEMENTS

This study was supported by the Spanish government MEC under Grants No: MAT2013-46649-C4-3-P, MAT2013-46649-C4-2-P, MAT2010-21270-C04-03/04 and CTQ2009-14596-C02-01, by MALTA Consolider Ingenio 2010 project (CSD2007-00045) and by Generalitat Valenciana (GVA-ACOMP-2013-1012). A.M., and P.R-H. acknowledge computing time provided by Red Española de Supercomputación (RES) and MALTA-Cluster, and also to S. Muñoz-Rodríguez for providing a data-parsing application. J. A. S. acknowledges Juan de la Cierva fellowship program for financial support.

REFERENCES

[1] Bernard, J.E.; Zunger, A. Ordered-Vacancy Compound Semiconductors – Pseudocubic CdIn2Se4. *Phys. Rev. B* **1988**, *37*, 6835-6856.

[2] Badikov, V.V.; Kuzmin, N.V.; Laptev, V.B.; Malinovsky, A.L.; Mitin, K.V.; Nazarov, G.S.; Ryabov, E.A.; Seryogin, A.M.; Shchebetova, N.I. A Study oft he Optical and Thermal Properties of Non-linear Mercury Thiogallate Crystals. *Quantum Electron*. **2004**, *34*, 451-456.

[3] Georgobiani, A.N.; Radautsan, S.I.; Tiginyanu, I.M. Wide-Gap AB2C4 Semiconductors – Optical and Photoelectric Properties, and Potential Applications. *Sov. Phys. Sem.* **1985**, *19*, 121-132.

[4] Burlakov, I.I.; Raptis, Y.; Ursaki, V.V.; Anastassakis, E.; Tiginyanu, I.M. Order-Disorder Phase Transition in CdAl2S4 under Hydrostatic Pressure. *Solid State Commun.* **1997** *101*, 377-381.

[5] González, J.; Rico, R.; Calderón, E.; Quintero, M.; Morocoima, M. Absorption Edge of MnGa2Se4 Single Crystals under Hydrostatic Pressure. *Phys. Status Solidi B* **1999**, *211*, 45-49.

[6] Ursaki, V.V.: Burlakov, I.I.; Tiginyanu, I.M.; Raptis, Y.S.; Anastassakis, E.; Anedda, A. Phase Transitions in Defect Chalcopyrite Compounds under Hydrostatic Pressure. *Phys. Rev. B* **1999**, *59*, 257-268.

[7] Fuentes-Cabrera, M.; Sankey, O.F. Theoretical Study of the Ordered-Vacancy Semiconducting Compound CdAl2Se4. *J. Phys.: Condens. Matter* **2001**, *13*, 1669-1684.

[8] Fuentes-Cabrera, M. Ab Initio Study of the Vibrational and Electronic Properties of CdGa2S4 and CdGa2Se4 under Pressure. *J. Phys.: Condens. Matter* **2001**, *13*, 10117-10124.

[9] Grzechnik, A.; Ursaki, V.V.; Syassen, K.; Loa, I.; Tiginyanu, I.M.; Handfland, M. Pressure-Induced Phase Transitions in Cadmium Thiogallate CdGa2Se4. *J. Solid State Chem*. **2001**, *160*, 205-211.

[10] Mitani, T.; Onari, S.; Allakhverdiev, K.; Gashimzade, F.; Kerimova, T. Raman Scattering in CdGa2S4 under Pressure. *Phys. Stat. Sol. B* **2001***, 223*, 287-291.

[11] Tatsi, A.; Lampakis, D.; Liarokapis, E.; López, S.A.; Martínez, L.; Giriat, W. Pressure Effects in Phonon Modes and Structure of AB2C4 Compounds and Combinations. *High Press. Res*. **2002**, *22*, 89-93.

[12] Tiginyanu, I.M.; Ursaki, V.V.; Manjón, F.J.; Tezlevan, V.E. Raman Scattering Study of Pressure-Induced Phase Transitions in AB2C4 Defect-Chalcopyrites and Spinels. *J. Phys. Chem. Solids* **2003**, *64*, 1603-1607.

[13] Mitani, T.; Naitou, T.; Matsuishi, K.; Onari, S.; Allakhverdiev, K.; Gashimzade, F.; Kerimova, T. Raman Scattering in CdGa2Se4 under Pressure. *Phys. Stat. Sol. B* **2003**, *235*, 321-325.

[14] Allakhverdiev, K.; Gashimzade, F.; Kerimova, T.; Mitani, T.; Naitou, T.; Matsuishi, K.; Onari, S. Raman Scattering under Pressure in ZnGa2Se4. *J. Phys. Chem. Solids* **2003**, *64*, 1597-1601.

[15] Marquina, J.; Power, Ch.; Grima, P.; Morocoima, M.; Quintero, M.; Couzinet, B.; Chervin, J.C.; Munsch, P.; González, J. Crystallographic Properties of the MnGa2Se4 Compound under High Pressure. *J. Appl. Phys*. **2006**, *100*, 093513.

[16] Meenakshi, S.; Vijyakumar, V.; Godwal, B.K.; Eifler, A.; Orgzall, I.; Tkachev, S.; Hochheimer, H.D. High-Pressure X-ray Diffraction Study of CdAl2Se4 and Raman Study of AAl2Se4 (A=Hg, Mn) and CdAl2X4 (X=Se,S). *J. Phys. Chem. Solids* **2006**, *67*, 1660-1667.

[17] Errandonea, D.; Kumar, R.S.; Manjón, F.J.; Ursaki, V.V.; Tiginyanu, I.M. High-Pressure X-ray Diffraction Study on the Structure and Phase Transitions of the Defect-Stannite ZnGa2Se4 and Defect-Chalcopyrite CdGa2S4. *J. Appl. Phys.* **2008**, *104*, 063524.

[18] Meenakshi, S.; Vijyakumar, V.; Eifler, A.; Hochheimer, H.D. Pressure-Induced Phase Transition in Defect-Chalcopyrites HgAl2Se4 and CdAl2S4. *J. Phys. Chem. Solids* **2010***, 71*, 832-835.

[19] Singh, P.; Sharma, M;. Verma, U.P.; Jensen, P. Pressure Effects on Energy Gaps and Phase Transitions in ZnAl2Se4. *Z. Kristallogr.* **2010**, *225*, 508-513.

[20] Manjón, F.J.; Gomis, O.; Rodríguez-Hernández, P.; Pérez-González, E.; Muñoz, A.; Errandonea, D.; Ruiz-Fuertes, J.; Segura, A.; Fuentes-Cabrera, M.; Tiginyanu, I.; Ursaki, V.V. Nonlinear Pressure Dependence of the Direct Band Gap in Adamantine Ordered-Vacancy Compounds. *Phys. Rev. B* **2010**, *81*, 195201.

[21] Verma, U.P.; Singh, P.; Jensen, P. A Study of the Electronic, Optical and Thermal Properties for ZnAl2Se4 using the FP-LAPW Method. *Phys. Status Solidi B* **2011**, *248*, 1682-1689.

[22] Gomis, O.; Vilaplana, R.; Manjón, F.J.; Pérez-González, E.; López-Solano, J.; Rodríguez-Hernández, P.; Muñoz, A.; Errandonea, D.; Ruiz-Fuertes, J.; Segura, A.; Santamaría-Pérez, D.; Tiginyanu, I. M.; Ursaki, V.V. High-Pressure Optical and Vibrational Properties of CdGa2Se4: Order-Disorder Processes in Adamantine Compounds. *J. Appl. Phys*. **2012**, *111*, 013518.

[23] Gomis, O.; Vilaplana, R.; Manjón, F.J.; Santamaría-Pérez, D.; Errandonea, D.; Pérez-González, E.; López-Solano, J.; Rodríguez-Hernández, P.; Muñoz, A.; Tiginyanu, I.M.; Ursaki, V.V. Crystal Structure of HgGa2Se4 under Compression. *Mat. Res. Bull.* **2013**, *48*, 2128-2133.

[24] Gomis, O.; Vilaplana, R.; Manjón, F.J.; Santamaría-Pérez, D.; Errandonea, D.; Pérez-González, E.; López-Solano, J.; Rodríguez-Hernández, P.; Muñoz, A.; Tiginyanu, I.M.; Ursaki, V.V. High-Pressure Study of the Structural and Elastic Properties of Defect-Chalcopyrite HgGa2Se4. *J. Appl. Phys.* **2013**, 113, 073510.

[25] Vilaplana, R.; Robledillo, M.; Gomis, O.; Sans, J.A.; Manjón, F.J.; Pérez-González, E.; Rodríguez-Hernández, P.; Muñoz, A.; Tiginyanu, I.M.; Ursaki, V.V. Vibrational Study of HgGa2S4 under Pressure. *J. Appl. Phys*. **2013**, *113*, 093512.

[26] Vilaplana, R.; Gomis, O.; Pérez-González, E.; Ortiz, H.M.; Manjón, F.J.; Rodriguez-Hernandez, P.; Muñoz, A.; Alonso-Gutiérrez, P.; Sanjuán, M.L.; Ursaki, V.V.; Tiginyanu, I.M. Thermally Activated Cation Ordering in ZnGa2Se4 Single Crystals Studied by Raman Scattering, Optical Absorption, and Ab Initio Calculations. *J. Phys.: Condens. Matter* ***2013,*** 25, 165802.

[27] Vilaplana, R.; Gomis, O.; Pérez-González, E.; Ortiz, H.M.; Manjón, F.J.; Muñoz, A.; Alonso-Gutiérrez, P.; Sanjuán, M.L.; Ursaki, V.V.; Tiginyanu, I.M. High-Pressure Raman Scattering Study of Defect-Chalcopyrite and Defect-Stannite ZnGa2Se4. *J. Appl. Phys*. **2013**, *113*, 233501.

[28] Vilaplana, R.; Gomis, O.; Manjón, F.J.; Ortiz, H.M.; Pérez-González, E.; López-Solano, J.; Rodríguez-Hernández, P.; Muñoz, A.; Errandonea, D.; Ursaki, V.V; Tiginyanu. I.M. Lattice Dynamics Study of HgGa2Se4 at High Pressures. *J. Phys. Chem. C.* **2013**, *117*, 15773-15781.

[29] Errandonea, D.; Kumar, R. S.; Gomis, O.; Manjón, F. J.; Ursaki, V. V.; Tiginyanu, I. M. X-ray Diffraction Study on Pressure-Induced Phase Transformations and the Equation of State of ZnGa2Te4. *J. Appl. Phys.* ***2013****, 114,* 233507.

[30] Gomis, O.; Santamaría-Pérez, D.; Vilaplana, R.; Luna, R.; Sans, J.A.; Manjón, F.J.; Errandonea, D.; Pérez-González, E.; Rodríguez-Hernández, P.; Muñoz, A.; Tiginyanu, I.M.; Ursaki, V.V. Structural and Elastic Properties of Defect-Chalcopyrite HgGa2S4 under High Pressure. *J. Alloys Compds.* **2014**, *583*, 70-78.

[31] Sans, J. A.; Santamaría-Pérez, D.; Popescu, C.; Gomis, O.; Manjón, F. J.; Vilaplana, R.; Muñoz, A.; Rodríguez-Hernández, P.; Ursaki, V.V.; Tiginyanu, I. M. Structural and Vibrational Properties of CdAl2S4 under High Pressure: Experimental and Theoretical Approach. *J. Phys. Chem. C*, **2014***, 118*, 15363-15374.

[32] Manjón, F.J.; Vilaplana, R.*, in Pressure-induced phase transitions in AB_2X_4 chalcogenide compounds*, Springer Series in Materials Science **189**, ed. by F.J. Manjón, I. Tiginyanu and V. Ursaki (Springer, Berlin, 2014), pp. 133-161.

[33] Gomis, O.; Manjón, F.J.*, in Pressure-induced phase transitions in AB_2X_4 chalcogenide compounds*, Springer Series in Materials Science **189**, ed. by F.J. Manjón, I. Tiginyanu and V. Ursaki (Springer, Berlin, 2014), pp. 163-184.

[34] Muñoz A.; Fuentes-Cabrera, M.*, in Pressure-induced phase transitions in AB_2X_4 chalcogenide compounds*, Springer Series in Materials Science **189**, ed. by F.J. Manjón, I. Tiginyanu and V. Ursaki (Springer, Berlin, 2014), pp. 185-210.

[35] Hahn, H.; Frank, G.; Klingler, W.; Storger, A.; Storger, G. Untersuchungen uber Ternare Chalkogenide. 6. Uber Ternare Chalkogenide des Aluminiums, Galliums und Indiums mit Zink, Cadmium und Quecksilber. *Z. Anorg. Allg. Chem.* **1955**, *279*, 241-270.

[36] Koval, L.S.; Stanchu, A.V.; Sobolev, V.V.; Radautsan, S; Markus, M.M. Optical Properties of 2 Modifications of CdIn2Se4. *Phys. Status Solidi A* **1972**, *9*, K69-K69.

[37] Przedmojski, J.; Palosz. B. X-ray Investigation of Needle-like Crystals of CdIn2Se4. *Phys. Stat. Sol. A* **1979**, *51*, K1-K1.

[38] Manolikas, C.; Bartzokas, D.; Vantendeloo, G.; Vanlanduyt. High-Resolution Electron-Microscopic Study of Polytypism in CdIn2Se4. *Phys. Stat. Sol. A* **1980**, *59*, 425-436.

[39] Haeuseler, H. FIR and Raman Spectra of Ternary Chalcogenides of Gallium and Indium with Zinc, Cadmium and Mercury. *J. Solid State Chem.* **1978**, 26, 367-376.

[40] Neumann, H.; Kissinger, W.; Levy, F.; Sobotta H.; Riede, V. Infrared Lattice-Vibrations of CdIn2Se4. *Cryst. Res. Technol.* **1990**, 25, 1455-1459.

[41] Razzetti, C.; Lottici, P.P. Raman Scattering in Defective AB2X4 Compounds and Alloys. *Jpn. J. Appl. Phys.* **1993**, 32, Supp. 32-3, 431-435.

[42] Attolini, G.; Bini, S.; Lottici, P.P.; Razzetti, C. Effects of Group-III Cation Substitution in the Raman Spectra of some Defective Chalcopyrites. *Cryst. Res. Technol*. **1992**, *27*, 685-690.

[43] Bärnighausen, H. Group-Subgroup Relations between Space Groups: A Useful Tool in Crystal Chemistry. *MATCH, Commun. Math. Chem*. **1980**, *9*, 139-175.

[44] Range, K.J.; Becker, W.; Weiss, A. Properties of CdIn2Se4 at High Pressure. *Z. Naturforschg.* **1969**, 24b, 1654.

[45] Range, K.J. Hochdruckuntersuchungen an Ternaren Chalkogeniden mit Tetraedrisch Koordinierten Kationen. *Chem. Zeit.* **1971**, 95, 3-11.

[46] Marinelli, M.; de Pascale, T.M.; Meloni, F.; Mula, G.; Serra M.; Baroni, S. Theoretical Study of Cubic vs Tetragonal Structures of Defect Zincblende Semiconductors – CdIn2Se4. *Phys. Rev. B* **1989**, 40, 1725-1731.

[47] Tiginyanu, I.M.; Modovyan, N.A.; Stoika, O.D. Phonon-Spectrum and Band Edge Absorption in CdAl2S4. *Fiz. Tverd. Tela* **1992**, *34,* 967-969.

[48] Fauth, F.; Peral, I.; Popescu, C.; Knapp, M. The New Material Science Powder Diffraction Beamline at ALBA Synchrotron. *Powd. Diffract.* **2013**, 28, S360-S370.

[49] Hammersley, A. P.; Svensson, S. O.; Hanfland, M.; Fitch, A. N.; Hausermann, D. Two-Dimensional Detector Software: From Real Detector to Idealized Image or Two-Theta Scan. *High Press. Res.* **1996**, *14*, 235-248.

[50] Klotz, S.; Chervin, J. C.; Munsch, P.; Le Marchand, G. Hydrostatic Limits of 11 Pressure Transmitting Media. *J. Phys. D: Appl. Phys*. **2009**, *42*, 075413.

[51] Dewaele, A.; Loubeyre, P.; Mezouar, M. Equations of State of Six Metals above 94 GPa. *Phys. Rev. B* **2004**, *70*, 094112.

[52] Laugier, J.; Bochu, B., LMGP-Suite Suite of Programs for the interpretation of X-ray Experiments, ENSP/Laboratoire des Matériaux et du Génie Physique, France. http://www.inpg.fr/LMGP and http://www.ccp14.ac.uk/tutorial/lmgp/

[53] Nolze, G.; Kraus, W. Powdercell 2.0 for Windows *Powd. Diffr.* **1998**, *13*, 256-259.

[54] Rodriguez-Carvajal, J. Recent Advances in Magnetic-Structure Determination by Neutron Powder Diffraction. *Physica B* **1993**, *192*, 55-69.

[55] Mao, H. K.; Xu, J.; Bell, P. M. Calibration of the Ruby Pressure Gauge to 800-Kbar under Quasi-Hydrostatic Conditions. *J. Geophys. Res.-Solid Earth Planets* **1986**, *91*, 4673-4676.

[56] Choe, S.H.; Park, B.N.; Yu, K.S.; Oh, S.J.; Park, H.L.; Kim, W.T. Optical Properties of Undoped and Co-Doped CdIn2Se4 Single-Crystals. *J. Phys. Chem. Solids* **1995**, *56*, 89-92.

[57] Hohenberg, P.; Kohn, W. Inhomogeneous Electron Gas. *Phys. Rev..B* **1964,** *136*, 864-871.

[58] Kresse, G.; Hafner, J. Ab Initio Molecular-Dynamics for Liquid Metals. *Phys. Rev. B* **1993**, *47*, 558-561.

[59] Kresse, G.; Hafner, J. Ab Initio Molecular-Dynamics Simulation of the Liquid Metal Amorphous-Semiconductor Transition in Germanium. *Phys. Rev. B* **1994**, *49*, 14251-14269.

[60] Kresse, G.; Furthmuller, J. Efficiency of Ab-Initio Total Energy Calculations for Metals and Semiconductors using a Plane-Wave Basis Set. *Comput. Mater. Sci.***1996**, *6*, 15-50.

[61] Kresse, G.; Furthmuller, J. Efficient Iterative Schemes for Ab Initio Total-Energy Calculations using a Plane-Wave Basis Set. *Phys. Rev. B* **1996**, *54*, 11169-11186.

[62] Blochl, P.E. Projector Augmented-Wave Method. *Phys. Rev. B* **1994**, *50*, 17953-17979.

[63] Kresse, G.; Joubert, D. From Ultrasoft Pseudopotentials to the Projector Augmented-Wave Method. *Phys. Rev. B* **1999**, *59*, 1758-1775.

[64] Perdew, J.P.; Ruzsinszky, A.; Csonka, G.I.; Vydrov, O.A.; Scuseria, G.E.; Constantin, L.A.; Zhou, X.L.; Burke, K. Restoring the Density-Gradient Expansion for Exchange in Solids and Surfaces. *Phys. Rev. Lett*. **2008**, *100*, 136406.

[65] Mujica, A.; Rubio, A.; Muñoz, A.; Needs, R. High-Pressure Phases of Group IV, III-V, and II-VI Compounds. *J. Rev. Mod. Phys.* **2003**, *75*, 863-912.

[66] Santamaria-Perez, D.; Amboage, M.; Manjón, F.J.; Errandonea, D.; Muñoz, A.; Rodriguez-Hernandez, P.; Mujica, A.; Radescu, S.; Ursaki, V.V.; Tiginyanu, I.M. Crystal Chemistry of CdIn2S4, MgIn2S4 and MnIn2S4 Thiospinels under High Pressure. *J. Phys. Chem. C* **2012**, *116,* 14078-14087.

[67] Parlinski, K.; Li, Z. Q.; Kawazoe, Y. First-Principles Determination of the Soft Mode in Cubic ZrO2. *Phys. Rev. Lett.* **1997**, *78*, 4063-4066.

[68] Lottici, P.P.; Antonioli, G.; Razzetti, C. Ordered-Vacancy Compound Semiconductors – An EXAFS Study of the Structure of Alpha-CdIn2Se4. *J. Phys. Chem. Solids* **1989**, *50*, 967-973.

[69] Birch, F. Finite Strain Isotherm and Velocities for Single Crystal and Polycrystalline NaCl at High-Pressures and 300 Degrees K. *J. Geophys. Res*. **1978***, 83*, 1257-1268.

[70] Kistaiah, P.; Satyanarayana Murthy, K.; Krishna Rao, K.V. X-ray Determination of the Lattice Parameter and Thermal Expansion of the Compound CdIn2Se4. *Phys. Status Solidi A* **1982**, 71, K225-K229.

[71] Santamaria-Perez, D; Gracia, L; Garbarino, G; Beltran, A; Chulia-Jordan, R; Gomis, O; Errandonea, D; Ferrer-Roca, C; Martinez-Garcia, D; Segura, A. High Pressure Study of the Behavior of Mineral Barite by X-ray Diffraction. *Phys. Rev. B* **2011**, *84*, 054102.

[72] Kroumova, E.; Arroyo, M.I.; Perez-Mato, J.M.; Kirov, A.; Capillas, C.; Ivantchev, S.; Wondratschek, H. Bilbao Crystallographic Server: Useful Databases and Tools for Phase-Transition Studies. *Phase Transitions* **2003**, *76*, 155-170.

[73] Canepa, P.; Hanson, R. M.; Ugliengo, P.; Alfredsson, M. J-ICE: A New Jmol Interface for Handling and Visualizing Crystallographic and Electronic Properties. *J. Appl. Cryst.* **2011**, *44*, 225-229.

[74] Muller, O.; Roy, R., *The Major Ternary Structural Families*, Springer Verlag, Berlin, **1974**.

[75] Zhang, X.; Zunger, A. Diagrammatic Separation of Different Crystal Structures of A2BX4 Compounds without Energy Minimization: A Pseudopotential Orbital Radii Approach. *Adv. Funct. Mater*. **2010**, *20*, 1944-1952.

Table I. Lattice parameters and atomic coordinates used to describe an atomic arrangement similar to that of the defect rocksalt-type structure. The splitting of the Wyckoff positions permits the space group Imma leave vacant ¼ of the cationic positions in an ordered and stoichiometric fashion. Occupation factors separated by slashes show the different combinations to place the vacant and cations. Cd and In atoms must maintain a stoichiometric ratio 1:2, as denoted in the $CdIn_2Se_4$ chemical formula.

	Fm-3m (No. 225) Z = 1				Fd-3m (No. 227) Z=8				Imma (No. 74) Z=4		
	a = 5.402 Å		Occ. factor		a' = 10.804 Å		Occ. factor		a'' ~ a'/√2 = 7.68 Å b'' ~ a'/√2 = 7.66 Å c'' ~ a' = 10.72 Å		Occ. factor
Cd	4a	(0, 0, 0)	0.25		16c	(0, 0, 0)	0.5/1		4a 4d	(0, 0, 0) (¼, ¼, ¾)	0/1/1/1 1/0/1/1
In	4a	(0, 0, 0)	0.5		16d	(½, ½, ½)	1/0.5		4b 4c	(0, 0, ½) (¼, ¼, ¼)	1/1/0/1 1/1/1/0
Se	4b	(½, ½, ½)	1		32e	(¼, ¼, ¼)	1		8h 8i	(0, -0.00017, 0.25082) (0.25158, ¼, -0.00914)	1 1

Table II. Unit-cell volume per formula unit at zero pressure (V_0) and bulk modulus (B_0) for the three phases observed in this study from 2nd order Birch-Murnaghan EOS fit. Previously reported experimental[44,70] and theoretical data[46] are shown for sake of comparison.

		V_0/Z (Å^3)	B_0 (GPa)	EOS-type
Phase I PS	Exp.	197.6(3)	41.1(9)	2nd-order BM
	Exp. (Ref. 71)	197.2		
	Theor.	196.6(2)	36.9(3)	2nd-order BM
	Theor. (Ref. 47)	173.5	49	Murnaghan
Phase II DR	Exp.	174(1)	57(3)	2nd-order BM
	Theor.	172.3(1)	55.5(4)	2nd-order BM
Phase III Spinel	Exp.	183(1)	-	-
	Exp. (Ref. 45)	182.3		
	Theor.	183.7(1)	63.9(3)	2nd-order BM
	Theor. (Ref. 47)	154.2	86	Murnaghan

Table III. Experimental bulk modulus (B_0), and its pressure derivative (B_0') at room pressure of sulphur- and selenium-based ternary OVCs. The pressure transmitting medium (PTM) used during the experiment is given.

Compound	B_0 (GPa)	B_0'	PTM	Ref.
DS-$ZnGa_2Se_4$	47(2)	3.9(3)	silicone oil	17
DC-$MnGa_2Se_4$[a]	44(2)	3.8(4)	methanol-ethanol, neon, and silicone oil	15
DC-$CdAl_2Se_4$	52.1	4 (fixed)	methanol-ethanol	16
DC-$CdGa_2Se_4$	41.5(2)	5(1)	methanol-ethanol	9
DC-$HgAl_2Se_4$	66(1.5)	4 (fixed)	paraffin oil	18
DC-$HgGa_2Se_4$	52(2) 39(2)	4 (fixed) 5.2(4)	MgO methanol-ethanol	23 24
PS-$CdIn_2Se_4$	41.1(9)	4 (fixed)	methanol-ethanol-water	This work
DC-$CdGa_2S_4$	64(2)	4.1(3)	silicone oil	17
DC-$CdAl_2S_4$	44.6(1) 41.2(2)	4 (fixed) 5.4	methanol-ethanol methanol-ethanol-water	18 31
DC-$HgGa_2S_4$	48.4(3)	4(fixed)	methanol-ethanol	30

[a] B_0 and B_0' parameters were obtained in Ref. 15 by means of a single EOS fit to data from three different experiments using each one of the three PTM indicated in the table.

Table IV. Experimental (exp.) and calculated (theor.) optical vibrational frequencies at room temperature and their pressure coefficients in PS-$CdIn_2Se_4$ as obtained from fits to the data using equation, $\omega = \omega_0 + a \cdot P + b \cdot P^2$. R, I, and IA mean Raman-active, Infrared-active and inactive, respectively.

Theor.				Exp.[a]				Exp.			
Mode symmetry	ω_0 (cm^{-1})	a (cm^{-1} GPa^{-1})	b (cm^{-1} GPa^{-2})	Mode symmetry	ω_0 (cm^{-1})	a (cm^{-1} GPa^{-1})	b (cm^{-1} GPa^{-2})	Mode symmetry	ω_0 [b] (cm^{-1})	ω_0 [c] (cm^{-1})	ω_0 [d] (cm^{-1})
E^1_{TO} (RI)	49.7	-1.12	-0.009					E	70	64	
E^1_{LO} (RI)	59.9	-0.30	-0.013								
A_2^1 (IA)	52.3	-1.20	-0.060					B_2	79	81	
$B_2{}^1_{TO}$(RI)	65.8	0.08	-0.055					E	[89]	92	
$B_2{}^1_{LO}$(RI)	65.8	0.08	-0.055								
E^2_{TO} (RI)	78.1	-0.59	0.026	E^2_{TO}	81.8(3)	-0.8(2)	0.04(4)	B_2	[124]		
E^2_{LO} (RI)	102.5	-0.50	0.004								
A_1^1 (R)	138.4	4.54	-0.002	A_1^1	139.6(3)	5.2(2)	-0.11(4)	A_1	141		
$B_2{}^2_{TO}$ (RI)	160.1	4.21	-0.088	$B_2{}^2_{TO}$	156.7(5)	3.5(4)	-0.01(6)	E	157	162	
$B_2{}^2_{LO}$ (RI)	167.0	3.89	-0.066					B_1	173		
E^3_{TO} (RI)	175.8	3.20	-0.024	E^3_{TO+LO}	189.7(6)	3.0(5)	-0.09(8)	B_2	182		
E^3_{LO} (RI)	176.1	3.00	0.004					A_1	188	191	186
E^4_{TO} (RI)	179.1	4.94	-0.091	E^4_{TO}	198.9(6)	5.1(5)	-0.17(7)				
E^4_{LO} (RI)	205.8	4.88	-0.119								
A_1^2 (R)	181.3	3.84	-0.073	$A_1^2 + B_1$	200.8(4)	3.8(3)	-0.17(4)				
B_1 (R)	183.3	3.37	-0.030					E	200		198
A_2^2(IA)	206.2	4.53	-0.087					E+B (TO)	218	220	213
E^5_{TO} (RI)	206.0	4.81	-0.097	E^5_{LO}	233.1(5)	4.4(4)	-0.13(6)				
E^5_{LO} (RI)	217.1	3.98	-0.071								
$B_2{}^3_{TO}$ (RI)	210.9	3.05	-0.043	$B_2{}^3_{LO}$	233.6(3)	1.0(2)	0.13(3)	E+B (LO)	238		239
$B_2{}^3_{LO}$ (RI)	219.2	3.11	-0.053								

[a] This work
[b] Raman data taken from Refs. 41 and 42
[c] IR data taken from Ref. 39
[d] IR data taken from Ref. 40

FIGURE CAPTIONS

Figure 1. **(Color online)** (a) Zinc-blende-type structure of CdSe. (b) Pseudocubic P-42m structure of $CdIn_2Se_4$ at ambient conditions. Vacancies are denoted as V. (c) Defect rocksalt-type structure of $CdIn_2Se_4$ at 8.7 GPa. (d) Spinel structure of $CdIn_2Se_4$ at ambient conditions after decompression.

Figure 2. (Color online) Bärnighausen tree of group–subgroup relations from ZB-type CdSe to $CdIn_2Se_4$. Every arrow pointing downwards points to a maximal subgroup and therefore corresponds to a reduction of symmetry. The letters *k* and *t* within the arrow followed by a number shows whether the subgroup is *klassengleich* or *translationengleich,* and the index of symmetry reduction. The origin shift is also given. Values in the boxes: element symbol, Wyckoff position, site symmetry and coordinates (*x, y, z)*.

Figure 3. (Color online) Selected X-ray powder diffraction patterns of $CdIn_2Se_4$ as a function of pressure. In all diagrams, the background was subtracted. The arrows indicate the appearance of new peaks corresponding to the DR phase at 7 GPa. Peaks of Cu (pressure gauge) are marked with asterisks. Observed, calculated, and difference profiles are depicted as black, red and blue lines. Vertical markers indicate Bragg reflections of the different phases.

Figure 4. (Color online) Volume-pressure data of the three phases observed in the study. Pseudocubic: squares, DR: circles, spinel: diamonds. Triangles represent the coexistence of DR

and spinel phases. Solid symbols denote upstroke data, whereas empty symbols denote downstroke data. Theoretically calculated data are represented as solid lines.

Figure 5. (Color online) (a) Calculated cation-anion and vacancy-anion distances, and (b) distance compressibilities as a function of pressure for the pseudocubic $CdIn_2Se_4$.

Figure 6. (Color online) Phonon dispersion curves and total and atom-projected one-phonon density of states of PS-$CdIn_2Se_4$ at ambient pressure.

Figure 7. (Color online) (a) Room temperature Raman scattering spectra of $CdIn_2Se_4$ at selected pressures up to 17.1 GPa on the upstroke and at 1 atm after releasing pressure and (b) Pressure dependence of the experimental (symbols) and calculated (lines) vibrational modes in PS-$CdIn_2Se_4$. Experimental A_1, B_1, B_2, and E modes are represented by solid triangles (red), solid circles (green), solid circles (blue), and solid squares (black), respectively. The same colours were used for the representation of theoretical calculations (lines) with the same symmetry. Solid (dashed) lines represent TO (LO) modes for the polar B_2 and E modes.

Figure 8. (Color online). Theoretical calculation of enthalpy difference vs. pressure for the initial PS, DR and spinel phases of $CdIn_2Se_4$. Enthalpy of PS phase is taken as the reference. Enthalpy is written per formula unit.

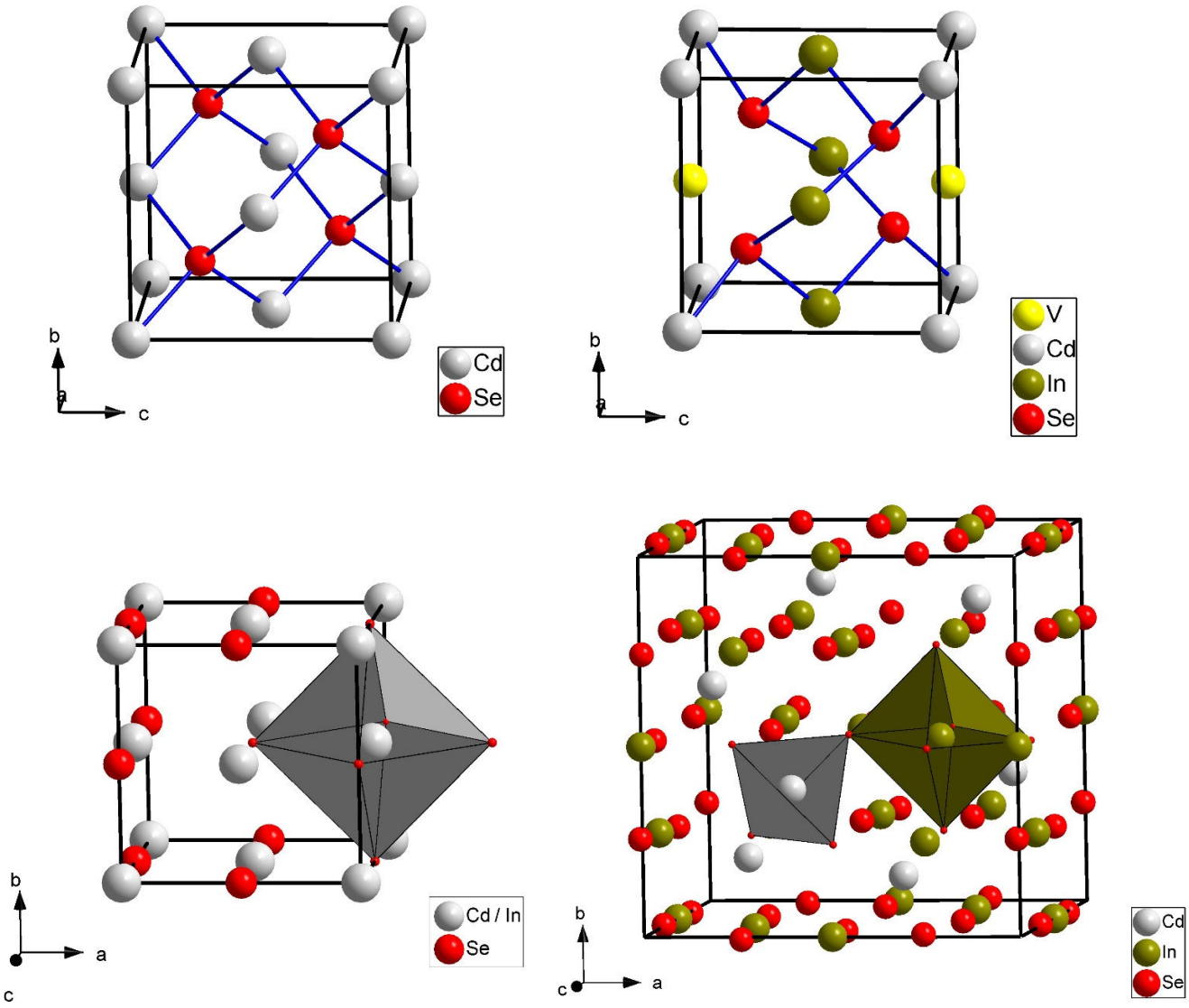

Figure 1

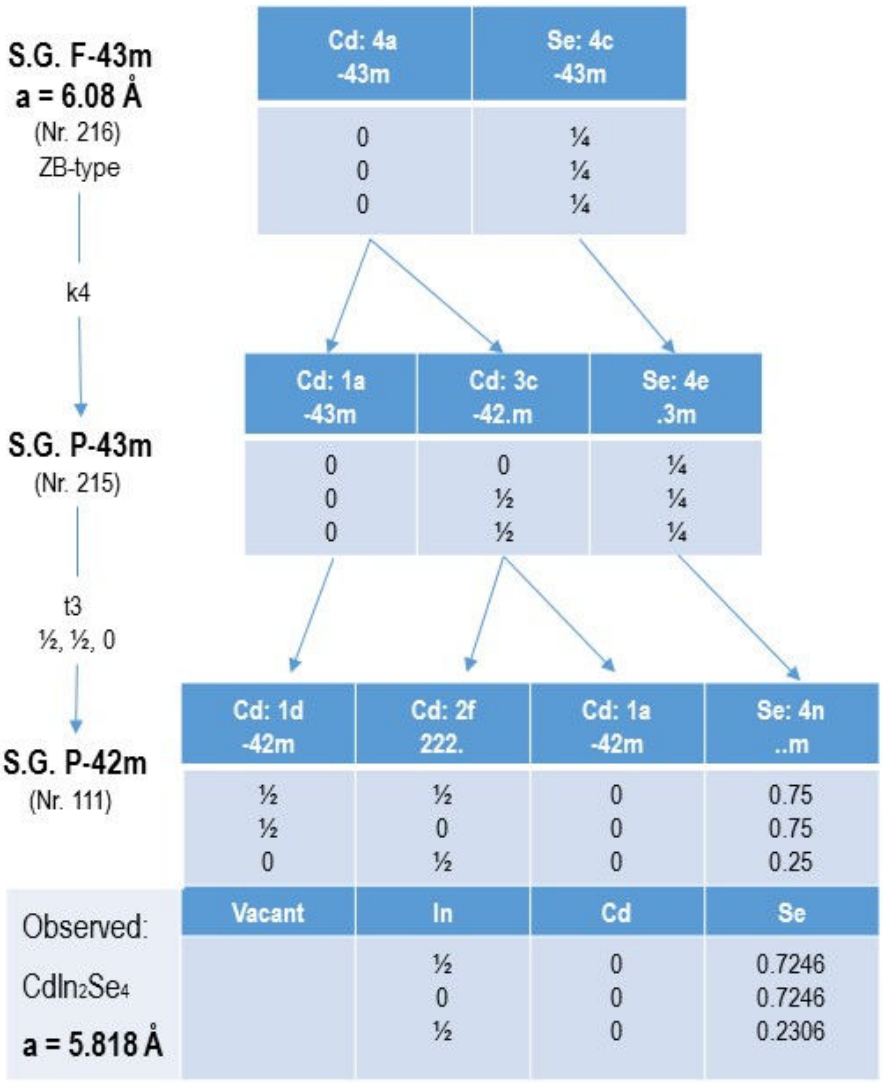
S.G. F-43m
a = 6.08 Å
(Nr. 216)
ZB-type
k4
S.G. P-43m
(Nr. 215)
t3
½, ½, 0
S.G. P-42m
(Nr. 111)
Observed:
CdIn2Se4
a = 5.818 Å
Cd: 4a -43m
Se: 4c -43m
0 0 0
¼ ¼ ¼
Cd: 1a -43m
Cd: 3c -42.m
Se: 4e .3m
0 0 0
0 ½ ½
¼ ¼ ¼
Cd: 1d -42m
Cd: 2f 222.
Cd: 1a -42m
Se: 4n ..m
½ ½ 0
½ 0 ½
0 0 0
0.75 0.75 0.25
Vacant
In
Cd
Se
½ 0 ½
0 0 0
0.7246 0.7246 0.2306

Figure 2.

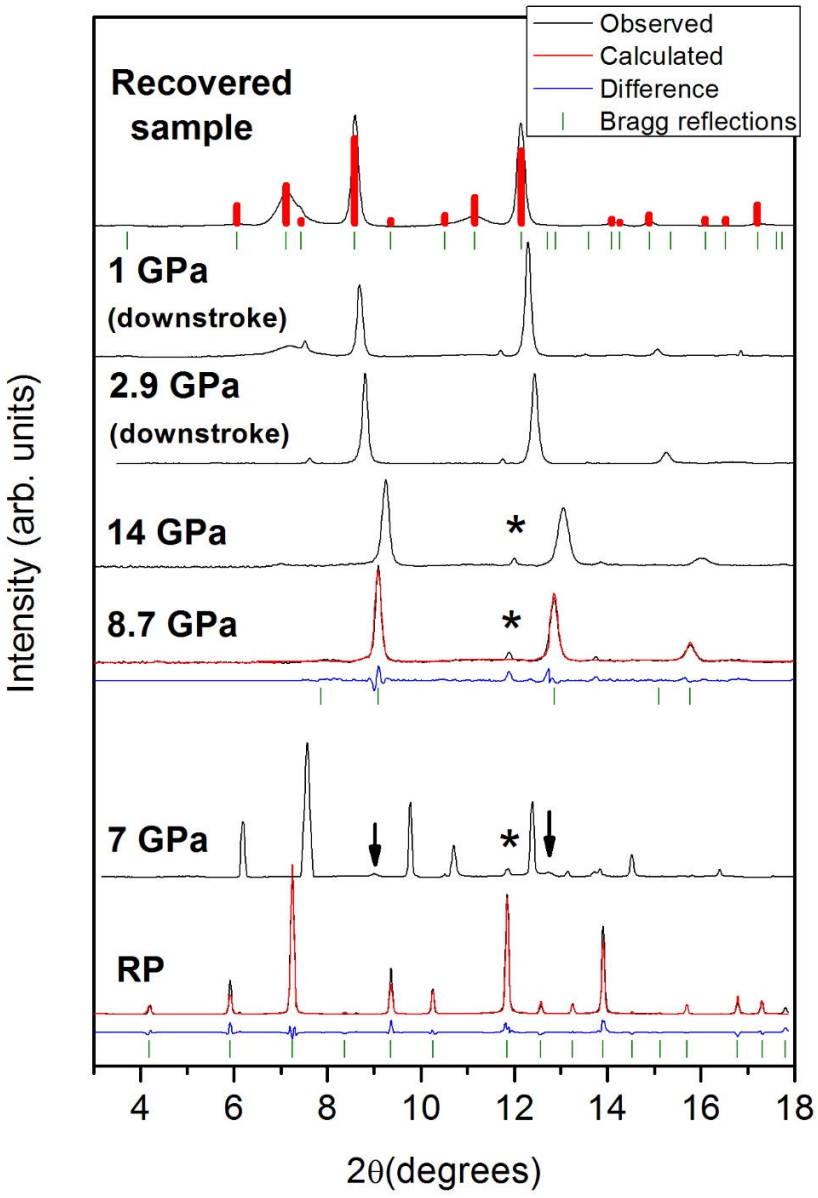
Observed
Calculated
Difference
Bragg reflections
Recovered sample
1 GPa
(downstroke)
2.9 GPa
(downstroke)
14 GPa
8.7 GPa
7 GPa
RP
*
Intensity (arb. units)
4
6
8
10
12
14
16
18
2θ(degrees)

Figure 3

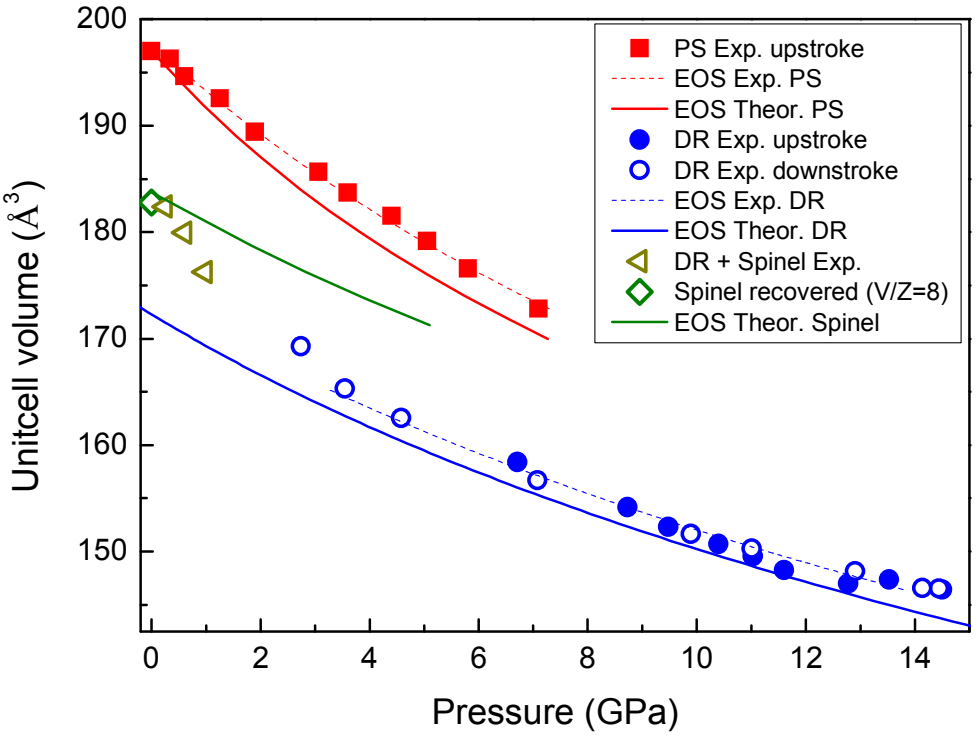
Unitcell volume (Å^3)
Pressure (GPa)
200
190
180
170
160
150
0
2
4
6
8
10
12
14
PS Exp. upstroke
EOS Exp. PS
EOS Theor. PS
DR Exp. upstroke
DR Exp. downstroke
EOS Exp. DR
EOS Theor. DR
DR + Spinel Exp.
Spinel recovered (V/Z=8)
EOS Theor. Spinel

Figure 4

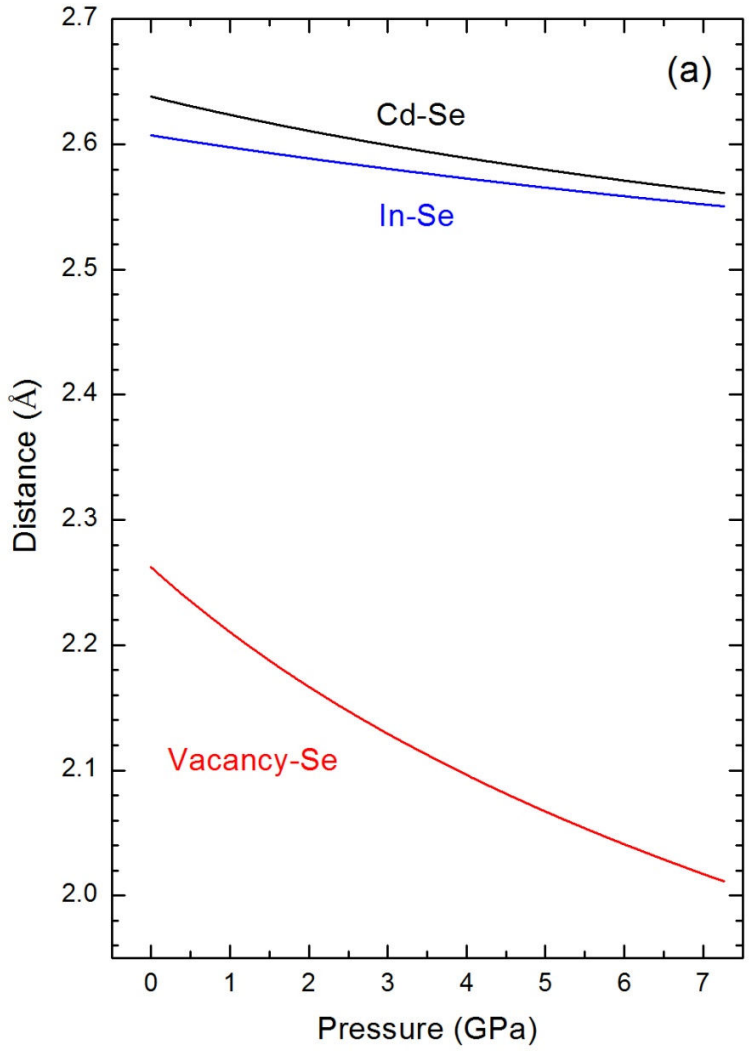
(a)
Cd-Se
In-Se
Vacancy-Se
Distance (Å)
Pressure (GPa)
2.7
2.6
2.5
2.4
2.3
2.2
2.1
2.0
0
1
2
3
4
5
6
7

Figure 5a

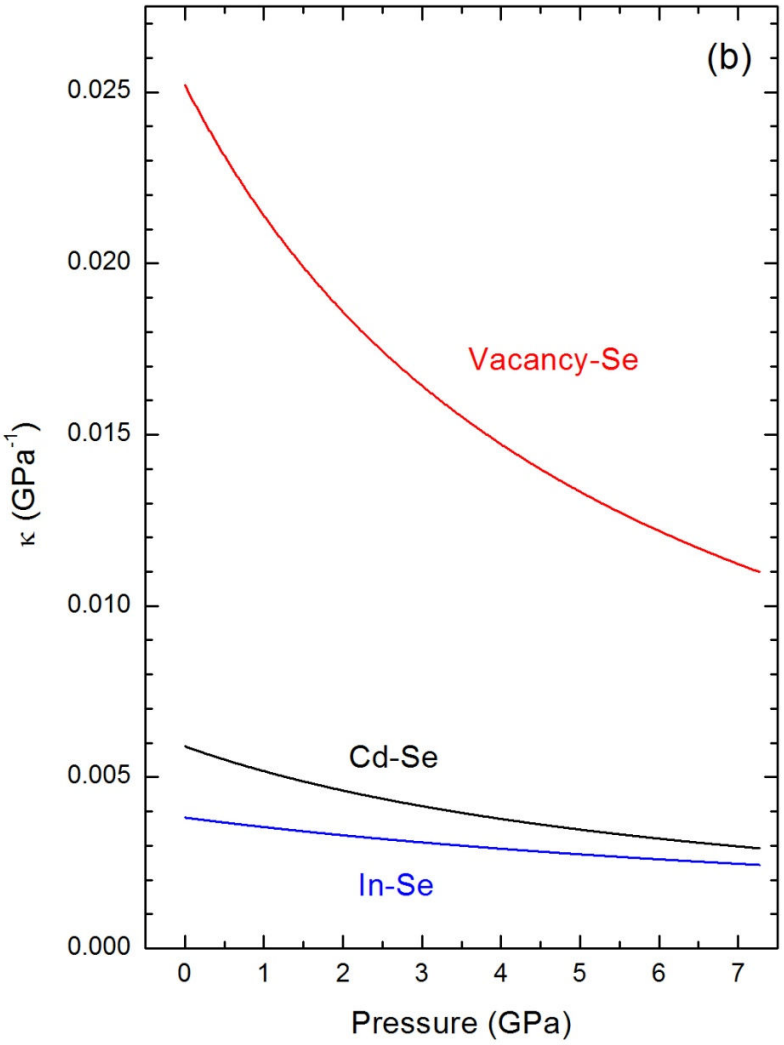
(b)
0.025
0.020
0.015
0.010
0.005
0.000
κ (GPa-1)
Vacancy-Se
Cd-Se
In-Se
0
1
2
3
4
5
6
7
Pressure (GPa)

Figure 5b

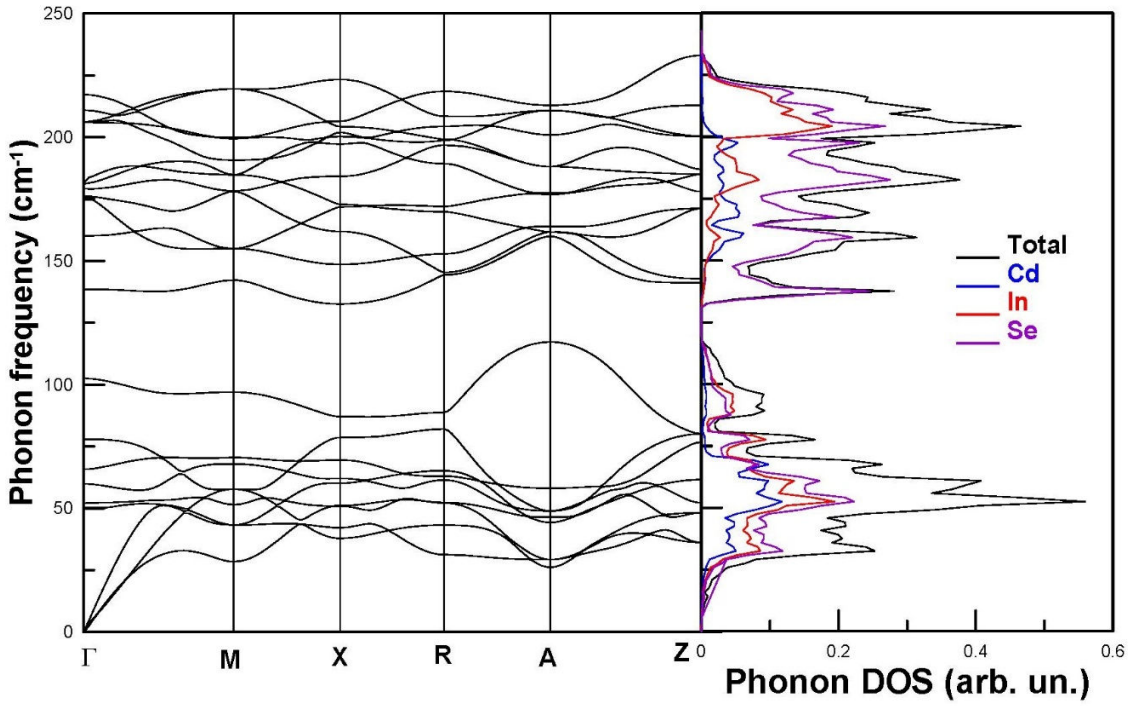
Phonon frequency (cm-1)
250
200
150
100
50
0
Γ
M
X
R
A
Z
0
0.2
0.4
0.6
Phonon DOS (arb. un.)
Total
Cd
In
Se

Figure 6.

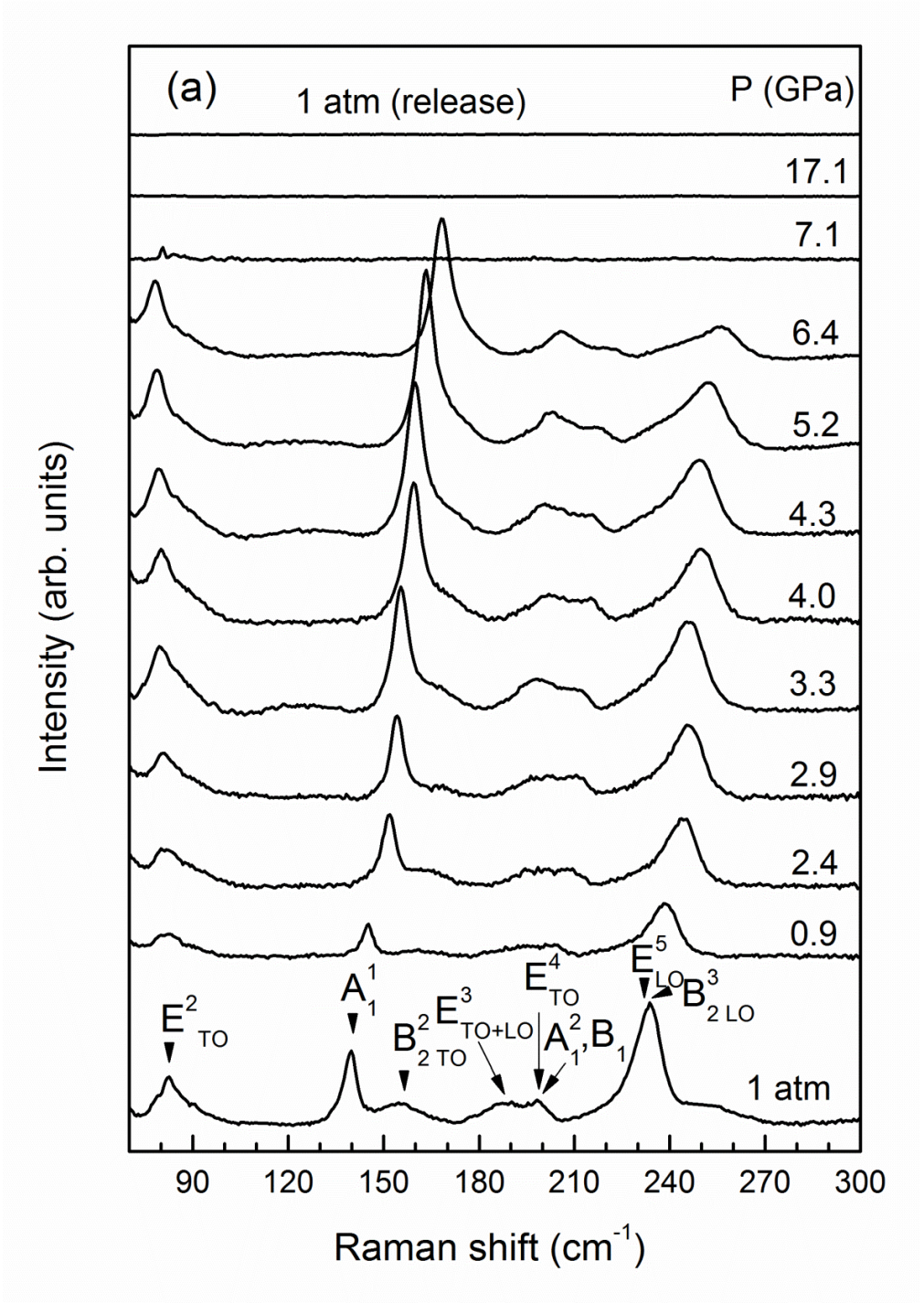
(a)
1 atm (release)
P (GPa)
17.1
7.1
6.4
5.2
4.3
4.0
3.3
2.9
2.4
0.9
1 atm
Intensity (arb. units)
Raman shift (cm-1)
90
120
150
180
210
240
270
300

Figure 7a

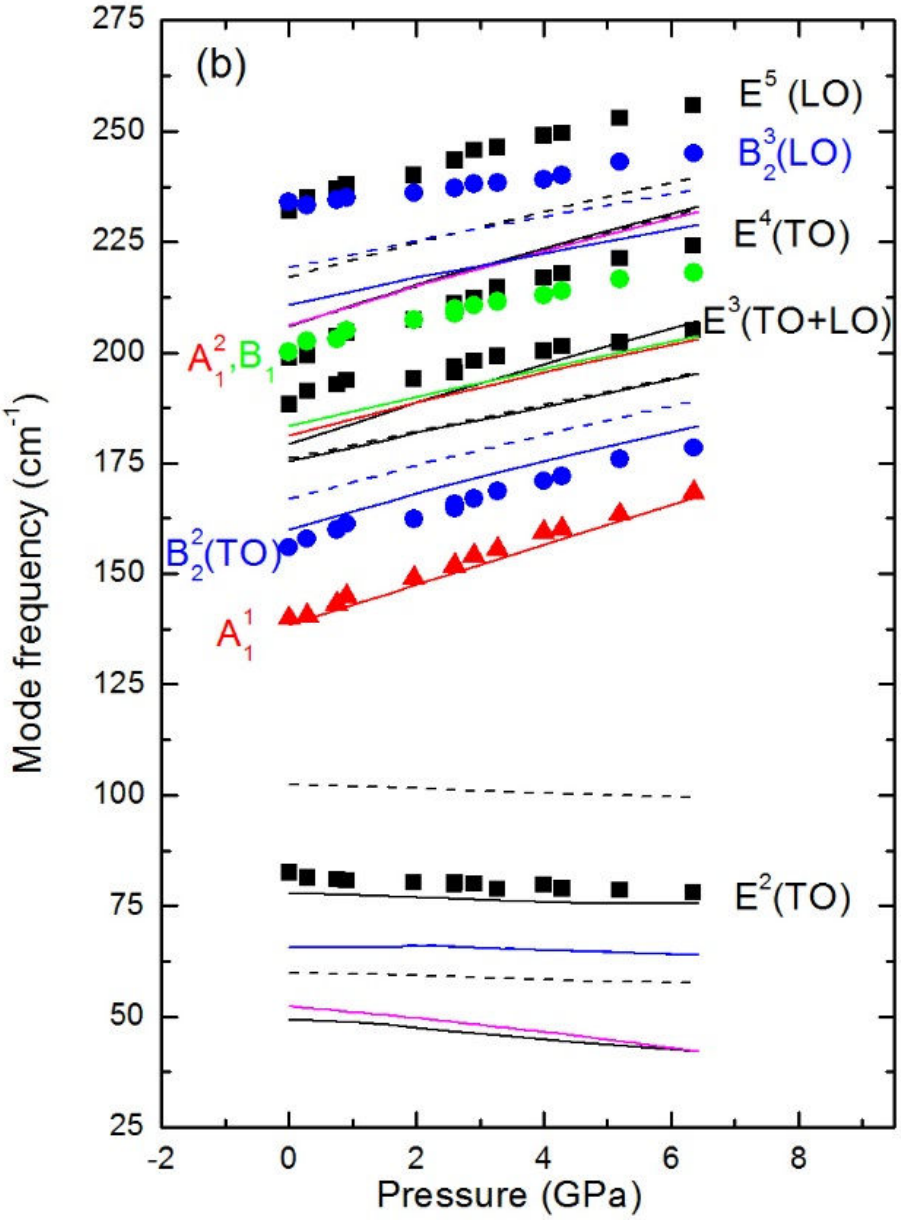
(b)
E5 (LO)
B23(LO)
E4(TO)
E3(TO+LO)
A12,B1
B22(TO)
A11
E2(TO)
Mode frequency (cm-1)
Pressure (GPa)
275
250
225
200
175
150
125
100
75
50
25
-2
0
2
4
6
8

Figure 7b

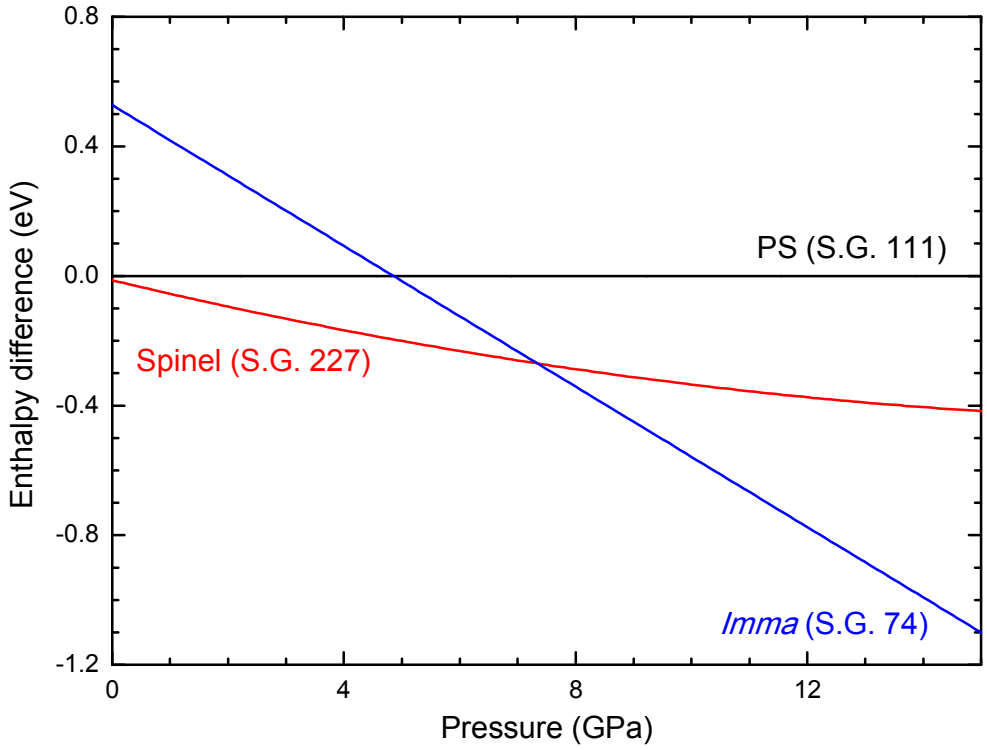
0.8
0.4
0.0
-0.4
-0.8
-1.2
Enthalpy difference (eV)
0
4
8
12
Pressure (GPa)
PS (S.G. 111)
Spinel (S.G. 227)
Imma (S.G. 74)

Figure 8.

SYNOPSIS

This experimental and theoretical study of pseudocubic $CdIn_2Se_4$ under compression evidences that this ordered-vacancy compound undergoes a phase transition at 7 GPa towards a disordered rocksalt structure. On decreasing pressure, at ~ 2 GPa, $CdIn_2Se_4$ transforms into a spinel structure which, according to calculations, is energetically competitive with the initial pseudocubic phase. Its phase behaviour and compressibility under compression is discussed.

TOC